An integral equation theory for polymer solutions: Explicit inclusion of the solvent molecules

Sergio Mendez
University of New Mexico, Albuquerque, New Mexico 87106

John G. Curro[a)]
Sandia National Laboratories, Albuquerque, New Mexico 87185

Mathias Pütz
Max Planck Institut for Polymer Research, Ackermannweg 10, Mainz, Germany

Dmitry Bedrov and Grant D. Smith
Department of Materials Science and Engineering and Department of Chemical and Fuels Engineering, University of Utah, Salt Lake City, Utah 84112

(Received 1 May 2001; accepted 5 July 2001)

Self-consistent Polymer Reference Interaction Site Model (PRISM) calculations and molecular dynamics (MD) simulations were performed on athermal solutions of linear polymers. Unlike most previous treatments of polymer solutions, we explicitly included the solvent molecules. The polymers were modeled as tangent site chains and the solvent molecules were taken to be spherical sites having the same intermolecular potential as the polymer sites. The PRISM theory was solved self-consistently for both the single chain structure and intermolecular correlations as a function of chain length and concentration. The rms end-to-end distance from PRISM theory was found to be in agreement with corresponding MD simulations, and exhibited molecular weight dependence in accordance with scaling predictions in the dilute and concentrated solution limits. The presence of explicit solvent molecules had a significant effect on the packing of the polymer by inducing additional structure in the intermolecular radial distribution function between polymer sites. Using the direct correlation functions from the athermal solution and the random phase approximation, we were able to estimate the spinodal curves for solutions when polymer and solvent attractions were turned on. We found significant deviations from Flory–Huggins theory that are likely due to compressibility and nonrandom mixing effects. © *2001 American Institute of Physics.*
[DOI: 10.1063/1.1397333]

I. INTRODUCTION

The modeling of polymers in solution has been a topic of great interest and activity among polymer scientists for many years starting with the pioneering work of Flory.[1] Noteworthy advances were subsequently made in dilute and concentrated solutions using perturbation theory,[2] self-consistent field theory,[3,4] and scaling theory.[5] Monte Carlo (MC),[6–8] as well as molecular dynamics (MD),[9] simulations have also proven to be invaluable to understanding how polymers behave in solution. Until recently, however, most of the work carried out on polymer solutions did not treat the solvent explicitly. Rather, the polymer solution was treated as a low density gas of polymers in a vacuum or in a continuum fluid. Our purpose in the present investigation is to model polymer solutions by explicitly including the effects of the solvent molecules on the equilibrium structure and thermodynamics of polymer solutions.

An explicit inclusion of solvent molecules in computer simulations of polymer solutions, especially dilute solutions, is challenging because (1) much of the computational effort is spent on the solvent thereby providing significantly poorer polymer statistics compared to concentrated solutions or polymer melts for the same computational effort, and (2) excluded volume and hydrodynamic screening that allows the use of relatively small periodic simulation cells for simulations of concentrated solutions and melts are not operative in dilute solutions. The latter effects necessitate the use of a larger simulation cell than is required for concentrated solutions and melts, further compounding the computational expense of dilute solution simulations. Despite these challenges, recent coarse-grained[10] and atomistic[11] simulations have been carried out on dilute polymer solutions. These simulations showed interesting polymer conformational effects as a function of solvent size and density.

Curro and Schweizer[12] developed a theory for polymers based on integral equation methods. This theory, called the *polymer reference interaction site model* or PRISM theory, has been successfully applied to polymer melts[13,14] and blends.[15,16] A number of studies[17–19] used PRISM theory self-consistently to compute the chain conformation of a polymer system as a function of concentration over the complete range from zero to melt densities. Solvent molecules were not explicitly accounted for in these computations. It was observed that the mean square end-to-end distance $\langle R_e^2 \rangle$ scaled as $N^{2\nu}$ where N is the number of monomeric units.

a)Electronic mail: jgcurro@sandia.gov

The Flory exponent ν changed from 3/5 at a low concentration of polymer to 1/2 at concentrations characteristic of the melt in agreement with scattering experiments, computer simulations and self-consistent field theory. Recently Khalatur and Khokhlov[20,21] employed self-consistent PRISM theory to treat the infinitely dilute solution of a polymer in an athermal monatomic solvent. They found that the Flory exponent was 3/5, characteristic of a good solvent, when the solvent diameter and monomer diameters were equal. Interestingly, they also observed the polymer chains to collapse when the solvent is much larger than the monomer size as in a polymer/colloid system. The infinitely dilute polymer solution was also recently treated with other integral equation theories in separate studies by Gan and Eu,[22] and Taylor and Lipson.[23]

In the current investigation, we employ self-consistent PRISM theory to study the conformation of polymers in solutions of a monatomic solvent. Here we study the conformation of polymers in solution as a function of concentration from dilute solutions to the melt. In addition, we carry out MD simulations on the same system of polymer and solvent at various concentrations. These simulations permit us to calibrate our PRISM solvation potential and to make detailed comparisons between theory and simulation for the polymer conformation and the intermolecular packing as a function of concentration. Furthermore, we are able to compare $\langle R_e^2 \rangle$ for our system (with solvent) with the corresponding chain dimensions for a single polymer chain in a vacuum.

Once we establish the intra and intermolecular structure of the athermal solution we then use this information to deduce the phase behavior when attractions are turned on (or the temperature is lowered). The Flory–Huggins theory[1] of polymer solutions has been remarkably successful in describing the miscibility behavior of solutions. However, as is well known, Flory–Huggins theory employed the dual approximations of incompressibility and random mixing. By contrast, PRISM theory includes both compressibility and nonrandom mixing effects. In this work we compare the PRISM theory with Flory–Huggins theory for the miscibility of polymer solutions to see the effect of these approximations.

We begin by briefly describing self-consistent PRISM theory, where in particular we introduce the solvation potential that represents the effects of the solvent molecules. We also describe our MD simulation techniques. We then compare the mean square end-to-end distance of the polymer chains from theory and simulation in the dilute solution, the 50/50 mixture, and the pure polymer melt for chain lengths of $N=10$, 20, 40, and 80. Finally we employ the random phase approximation (RPA) to compute the spinodal curves for various polymer solutions and chain lengths.

II. THEORY AND COMPUTATIONAL METHODOLOGY

A. Modeling the structure of the solution using PRISM theory

PRISM theory is an integral equation theory developed by Curro and Schweizer[12,24–26] as an extension to polymers of the reference interaction site model (RISM) theory of Chandler and Andersen.[27,28] In PRISM theory each molecule

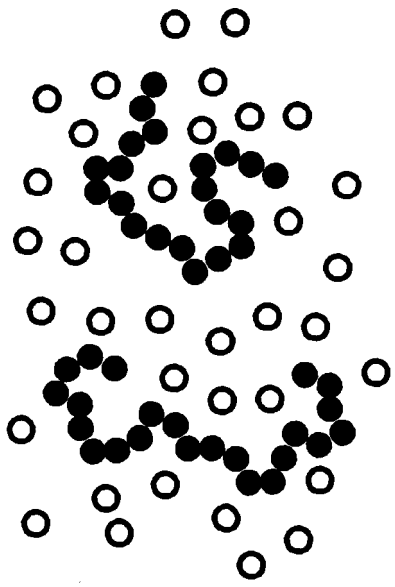

FIG. 1. Model of tangent site polymer chains immersed in solvent molecules.

is envisioned as a collection of spherically symmetric interaction sites (or beads) as depicted in Fig. 1. For simplicity the solvent molecules are modeled as single sites; more complex solvent architectures could be constructed from additional sites[28] if desired to model specific solvent molecules. All monomers of the chains are considered to be equivalent and end effects are neglected. The polymer and solvent molecules interact only through pairwise interactions between sites; no local nematic ordering is included in the model. For the case of polymers in solution, we seek to calculate the three independent *inter*molecular radial distribution functions, $g_{ss}(r)$, $g_{pp}(r)$, $g_{sp}(r)$, where s refers to solvent and p to polymer sites. The corresponding intermolecular direct correlation functions, $C_{ss}(r)$, $C_{pp}(r)$, $C_{sp}(r)$, can be defined through the generalized Ornstein–Zernike-type equation.[12,27,28] In Fourier transform space, this equation is

$$\hat{\mathbf{H}}(k)=\hat{\mathbf{\Omega}}(k)\cdot\hat{\mathbf{C}}(k)\cdot[\hat{\mathbf{\Omega}}(k)+\hat{\mathbf{H}}(k)], \tag{1}$$

where the overcaret denotes Fourier transformation with wave vector k. In real space, $C_{\alpha\gamma}(r)$ is the direct correlation function matrix and the matrix $H_{\alpha\gamma}(r)$ is defined in terms of the pair correlation functions as

$$H_{\alpha\gamma}(r)=\rho_\alpha\rho_\gamma[g_{\alpha\gamma}(r)-1], \tag{2}$$

where α and γ are s or p, and ρ_α is the density of sites of type α. The *intra*molecular structure of the single chain has the form

$$\hat{\Omega}_{pp}(k)=\frac{1}{N}\sum_{i,j}^{N}\left\langle\frac{\sin kr_{ij}}{kr_{ij}}\right\rangle, \tag{3}$$

with the summations i,j being taken over all sites on a single chain with N beads and the brackets indicate an ensemble average over all polymer chains. Since a solvent molecule consists of a single site, $\hat{\Omega}_{ss}(k)=1$; the cross term can be

shown to be $\hat{\Omega}_{sp}(k)=0$. We obtain the intramolecular structure from a single chain Monte Carlo simulation in a solvation potential discussed below.

Knowing the intramolecular $\hat{\Omega}_{\alpha\gamma}(k)$ matrix, we use Eq. (1) to solve for the intermolecular function $\hat{H}_{\alpha\gamma}(k)$. This can only be done by having a closure approximation for the direct correlation function matrix $\hat{C}_{\alpha\gamma}(k)$. We employ the well known Percus–Yevick (PY) approximation[12,29] for this purpose. In real space, its form is

$$C_{\alpha\gamma}(r)=\{1-\exp[\beta u^{\mathrm{rep}}_{\alpha\gamma}(r)]\}[H_{\alpha\gamma}(r)+1], \tag{4}$$

where $\beta=1/k_{\mathrm{B}}T$ and $u^{\mathrm{rep}}_{\alpha\gamma}(r)$ is the repulsive interaction potential between intermolecular sites α and γ. Only repulsive interactions are used since at high, liquid-like densities, it is well established[29] that the repulsive branch of the interaction potential determines the intermolecular packing $g_{\alpha\gamma}(r)$ in liquids. We decompose the full Lennard-Jones 6-12 potential following Weeks, Chandler, and Anderson[30] into a repulsive, reference part,

$$u^{\mathrm{rep}}_{\alpha\gamma}(r)=4\epsilon_{\alpha\gamma}\left[\left(\frac{\sigma_{\alpha\gamma}}{r}\right)^{12}-\left(\frac{\sigma_{\alpha\gamma}}{r}\right)^{6}+\frac{1}{4}\right], \quad r\leqslant\sigma_{\alpha\gamma}2^{1/6},$$
$$u^{\mathrm{rep}}_{\alpha\gamma}(r)=0, \quad r>\sigma_{\alpha\gamma}2^{1/6}, \tag{5a}$$

and an attractive, or perturbative, part,

$$u^{\mathrm{att}}_{\alpha\gamma}(r)=-\epsilon^{\mathrm{att}}_{\alpha\gamma}, \quad r<\sigma_{\alpha\gamma}2^{1/6},$$
$$u^{\mathrm{att}}_{\alpha\gamma}(r)=4\epsilon^{\mathrm{att}}_{\alpha\gamma}\left[\left(\frac{\sigma_{\alpha\gamma}}{r}\right)^{12}-\left(\frac{\sigma_{\alpha\gamma}}{r}\right)^{6}\right], \quad r\geqslant\sigma_{\alpha\gamma}2^{1/6}, \tag{5b}$$

where r is the distance between sites α and γ. $\epsilon_{\alpha\beta}$ and $\sigma_{\alpha\beta}$ are the usual Lennard-Jones parameters. It should be noted that $\epsilon^{\mathrm{rep}}_{\alpha\gamma}=\epsilon^{\mathrm{att}}_{\alpha\gamma}$ must hold in order for Eqs. (5a) and (5b) to add up to the full Lennard-Jones potential. We, however, approximate the perturbative part of the potential to have a separately controllable attractive parameter $\epsilon^{\mathrm{att}}_{\alpha\gamma}$ that will permit us to turn on an attractive potential independently without having to recompute the repulsive reference system.

For a given intramolecular structure function $\hat{\Omega}_{pp}(k)$, Eqs. (1) and (4) can be solved numerically to give the intermolecular pair correlation functions $g_{\alpha\gamma}(r)$. As a first approximation one could follow Flory's hypothesis[1] and determine $\hat{\Omega}_{pp}(k)$ for a melt of ideal chains with no long range excluded volume interactions. This is inadequate, however, for a polymer solution because excluded volume interactions are known to be important at lower concentrations of polymer. In fact, one would expect the intramolecular structure and the intermolecular packing to be coupled. Therefore, for our purposes we must solve the PRISM theory in a self-consistent manner for both the intra and intermolecular structure.[12–14,17–19] The first step of our iterative scheme involves finding $\hat{\Omega}_{pp}(k)$ through a Monte Carlo simulation. The total potential energy in the simulation is[12]

$$U(\underset{\sim}{R})=U_E+W_{pp}(\underset{\sim}{R}), \tag{6}$$

where $\underset{\sim}{R}$ represents the set of coordinates that define the instantaneous polymer conformation of the entire chain molecule. U_E is the sum of all pairwise, repulsive interactions $u^{\mathrm{rep}}_{\alpha\gamma}$ along the chain, and the N-body solvation potential, $W_{pp}(R)$, mimics the effect of the solvent acting on a chain. In order to make the problem tractable, we approximate the solvation potential to be pairwise additive and to have the form[12,31,32]

$$\beta\hat{W}_{pp}(k)=-K\sum_{i,j}\hat{C}_{pi}(k)\hat{S}_{ij}(k)\hat{C}_{jp}(k), \tag{7}$$

where the partial structure factors are defined as

$$\hat{S}_{\alpha\gamma}(k)=\rho_{\alpha}\hat{\Omega}_{\alpha\gamma}(k)+\hat{H}_{\alpha\gamma}(k). \tag{8}$$

The summations i and j in Eq. (7) are over polymer (p) and solvent (s) sites. Within our approximation, the same solvation potential $W_{pp}(r_{\alpha\gamma})$ acts between all intramolecular pairs of sites along the polymer backbone. As will be seen later in Sec. III, $W_{pp}(r_{\alpha\gamma})$ is attractive at short distances reflecting the fact that the other chains in the system tend to cause a given test macromolecule to contract. At larger distances, oscillations in the solvation potential due to packing of the solvent molecules are seen. The essence of the Flory ideality hypothesis[1] is that the repulsive excluded volume interactions and the medium induced attractions in Eq. (6) cancel each other out. Because of the approximate nature of the solvation potential we include a coefficient K in Eq. (7) that controls the overall strength of the field. Our strategy is to see if a constant value of K is adequate to capture the correct scaling behavior across the complete concentration range from the dilute solution to melt.

The first simulation in our iterative computational scheme can be performed with the initial guess of $W_{pp}(r)=0$ to calculate the first form of the intramolecular structure. At this point, one is able to solve the integral equations in Eqs. (1) and (4) for $\hat{H}_{\alpha\gamma}(k)$ and $\hat{C}_{\alpha\gamma}(k)$. With these functions, we can then calculate the static structure factor and solvation potential matrix from Eqs. (7) and (8). The newly calculated medium-induced potential is compared to the one used previously. If the difference between these two is greater than some predefined value, then we go into another iteration using an updated value of $\hat{W}_{pp}(k)$ in the Monte Carlo simulation. In this single chain simulation, the updated medium- induced potential is added to the repulsive Lennard-Jones interaction to define the total interaction between monomer sites. The solvation potential acts to compress the polymer chains whereas the repulsive potential causes expansion. This self-consistent iterative scheme, eventually, provides the correct balance of inter and intramolecular interactions, and thus yields both the equilibrium intramolecular structure $\hat{\Omega}_{pp}(k)$ and intermolecular pair correlation functions $g_{pp}(r)$, $g_{ss}(r)$, and $g_{sp}(r)$.

The single chain Monte Carlo simulations employ pivot moves made by randomly selecting a bond, then randomly rotating about the dihedral angle. Along with this pivot move, the bond angle is randomly varied between 0 and 40 degrees. The Monte Carlo moves are accepted or rejected according to Metropolis importance sampling.[33] Monte Carlo reweighing is used so that the simulation did not have to be repeated during each iteration step.[14,34]

B. Estimation of the spinodal curve from PRISM theory

The self-consistent PRISM theory we have outlined provides us with a complete description of the intra and intermolecular structure of the polymer solution. These structural calculations are carried out for the athermal reference system where we use the repulsive potential in Eq. (5a). We can use this information on the reference system to deduce the phase behavior of the polymer solution when the attractions are turned on. Curro and Schweizer[35] derived an exact expression for the spinodal condition of a compressible, binary system,

$$1-\rho_p N\hat{C}_{pp}(0)-\rho_s\hat{C}_{ss}(0)+\rho_p\rho_s N[\hat{C}_{pp}(0)\hat{C}_{ss}(0)-\hat{C}_{sp}^2(0)]=0, \tag{9}$$

written for the polymer solution case. For illustrative purposes, we make use of the random phase approximation (RPA),[29] valid for weak attractions, as a way of estimating how the direct correlation functions depend on the attractive parts of the potentials:

$$\begin{aligned}\hat{C}_{pp}(0)&\cong\hat{C}_{pp}^0-\beta\hat{u}_{pp}^{\mathrm{att}}(0),\\ \hat{C}_{ss}(0)&\cong\hat{C}_{ss}^0-\beta\hat{u}_{ss}^{\mathrm{att}}(0),\\ \hat{C}_{sp}(0)&\cong\hat{C}_{sp}^0-\beta\hat{u}_{sp}^{\mathrm{att}}(0);\end{aligned} \tag{10}$$

$\hat{C}_{\alpha\gamma}^0(0)$ is obtained for the athermal reference system by extrapolating to the zero wave vector. After some algebraic manipulations, we can express the spinodal temperature, T_S, as

$$k_{\mathrm{B}}T_s=\frac{-\hat{u}_{ss}^{\mathrm{att}}(0)\left(\frac{1}{\rho_pN}-\hat{C}_{pp}^0(0)\right)-\hat{u}_{pp}^{\mathrm{att}}(0)\left(\frac{1}{\rho_s}-\hat{C}_{ss}^0(0)\right)-2\hat{C}_{sp}^0(0)\hat{u}_{sp}^{\mathrm{att}}(0)}{\frac{1}{\rho_s\rho_pN}-\frac{\hat{C}_{ss}^0(0)}{\rho_pN}-\frac{\hat{C}_{pp}^0(0)}{\rho_s}+\hat{C}_{ss}^0(0)\hat{C}_{pp}^0(0)-\hat{C}_{sp}^0(0)^2}. \tag{11}$$

The Fourier transform of the attractive potential in Eq. (5b), $\hat{u}_{\alpha\gamma}^{\mathrm{att}}(0)$, can be found analytically in the zero wave vector limit:

$$\hat{u}_{\alpha\gamma}^{\mathrm{att}}(0)=4\pi\int_0^\infty r^2u_{\alpha\gamma}^{\mathrm{att}}(r)dr=\frac{-64\pi\epsilon_{\alpha\gamma}^{\mathrm{att}}\sigma_{\alpha\gamma}^3}{9\sqrt{2}}. \tag{12}$$

Substituting the above results into the previous equation for the spinodal temperature we obtain

$$k_{\mathrm{B}}T_S=\frac{64\pi\sigma^3}{9\sqrt{2}}\times\frac{\epsilon_{ss}^{\mathrm{att}}\left(\frac{1}{\rho_pN}-\hat{C}_{pp}^0\right)+\epsilon_{pp}^{\mathrm{att}}\left(\frac{1}{\rho_s}-\hat{C}_{ss}^0\right)+2\hat{C}_{sp}^0\epsilon_{sp}^{\mathrm{att}}}{\frac{1}{\rho_s\rho_PN}-\frac{\hat{C}_{ss}^0}{\rho_pN}-\frac{\hat{C}_{pp}^0}{\rho_s}+\hat{C}_{ss}^0\hat{C}_{pp}^0-\hat{C}_{sp}^{02}}, \tag{13}$$

where we take the Lennard-Jones σ's to be the same for both the polymer and the solvent.

From Eq. (13) it can be seen that once the direct correlation functions from the reference system are determined at the zero wave vector, the spinodal temperature T_S can be related to the solvent and polymer densities. The information regarding the packing of the solvent is contained in these direct correlation functions. In order to completely characterize the spinodal curve we must also have an equation of state for the mixture that relates ρ_p and ρ_s at constant pressure. For simplicity, we make the assumption that the volume change on mixing is zero. With this approximation we can write[15]

$$\rho_p=x\rho,\ \rho_s=(1-x)\rho,\qquad \frac{1}{\rho}=\frac{x}{\rho_p^0}+\frac{(1-x)}{\rho_s^0}, \tag{14}$$

where x is the site fraction of the polymer and ρ, ρ_p^0, ρ_s^0 are the densities of the solution, pure polymer, and pure solvent, respectively. Estimates based on a hard sphere equation-of-state for tangent site chains[36] suggest that the density of the monatomic solvent would be about 9% lower than the polymer density of $\rho_p^0=0.85\sigma^{-3}$ at constant pressure. In view of the already approximate nature of the calculation due to Eqs. (10) and (14), for illustrative purposes we make additional assumptions by taking the pure component densities of the polymer and solvent to be equal and maintain the overall density of the mixture fixed at $0.85\sigma^{-3}$ and by neglecting thermal expansion effects. It is important to recognize that the zero volume change of mixing approximation in Eq. (14) does not imply that the solution is incompressible. As an alternative, the volume change of mixing could be obtained from PRISM theory through the Kirkwood–Buff equations.[37]

If we impose the incompressibility constraint together with the random mixing approximation, one would expect the general RPA approximation in Eq. (13) to reduce to the Flory–Huggins result for the spinodal condition. For the case of random mixing, all the radial distribution functions are equal. This also implies that the direct correlation functions of the polymer and the solvent are also equal which leads to $\hat{C}_{pp}^0(0)=\hat{C}_{ss}^0(0)=\hat{C}_{sp}^0(0)$. The isothermal compressibility κ_T can be related to the direct correlation functions through the Kirkwood–Buff relations to give[35,37]

$$\frac{1}{\kappa_T} = k_B T \sum_{\alpha\gamma} \rho_\alpha \rho_\gamma \hat{S}^{-1}_{\alpha\gamma}(0). \tag{15}$$

For an incompressible system $\kappa_T = 0$ and Eq. (15), together with Eqs. (1) and (8), imply that $\hat{C}^0_{pp}(0) = \hat{C}^0_{ss}(0) = \hat{C}^0_{sp}(0) \to -\infty$. With these restrictions it can be seen that Eq. (13) reduces to

$$k_B T_S = \frac{64\pi\sigma^3\rho}{9\sqrt{2}} \frac{(\epsilon^{att}_{pp} + \epsilon^{att}_{ss} - 2\epsilon^{att}_{sp})}{[1/xN + 1/(1-x)]}. \tag{16}$$

This is indeed what the Flory–Huggins theory would predict for the spinodal condition of a polymer solution with a χ parameter suitably generalized to continuous space:

$$\chi = \frac{32\pi\sigma^3\rho}{9\sqrt{2}} \frac{(\epsilon^{att}_{pp} + \epsilon^{att}_{ss} - 2\epsilon^{att}_{sp})}{k_B T}. \tag{17}$$

C. Molecular dynamics simulations of polymer solutions

As part of this investigation, we also carry out MD simulations of infinitely dilute (1 polymer molecule per simulation box) and concentrated ($x = 0.5$) solutions using only the repulsive part of the Lennard-Jones (6-12) potential [Eq. (5a)] to describe $s-s$, $s-p$, and $p-p$ interactions. The polymer chains consist of N ($N = 10$, 20, 40, and 80) beads each of which is connected with neighboring beads by a bond of length of σ. Bond lengths are constrained during simulations using the SHAKE algorithm[38] while other intramolecular degrees of freedom are unrestricted resulting in a flexible freely-jointed representation of polymer chains. Solvent molecules are explicitly included in simulations as single beads that are identical to those that comprise the polymer chains. In simulations of infinitely dilute solutions a single polymer chain is dissolved in a large number of solvent molecules ($N_{\text{solvent}} \sim 7000$ for $N = 10$ and 20, and $N_{\text{solvent}} \sim 22\,000$ for $N = 40$ and 80) to avoid possible artifacts due to the correlation of a polymer molecule with its own image from periodic boundary conditions. For all systems at dilute solutions the ratio of the chain radius of gyration (R_g) to the simulation box length (L) is less than 0.17 which is lower than the acceptable limit for this ratio ($R_g/L \approx 0.2-0.3$) determined by Dunweg and Kremer[9] in their simulations of polymer solutions. For the concentrated solutions the systems contain 140–340 polymer chains and 3400–11 200 solvent molecules (depending on the length of the polymer chain). Simulations are performed in a NVT ensemble at density $\rho^* = \rho\sigma^3 = 0.85$ and temperature $T^* = k_B T/\epsilon = 1.0$. NVT conditions are implemented using the Nose–Hoover thermostat and explicit reversible integrators described elsewhere.[39] Production runs over $10.0-15.0 \times 10^6$ for (dilute solutions) and 2.0×10^6 (for concentrated solutions) integration time steps [$\Delta t = 0.001\tau$, where $\tau = \sigma(m/\epsilon)^{1/2}$] are conducted to sample conformational and structural properties of solutions after equilibrating each system over 2.0×10^6 integration steps.

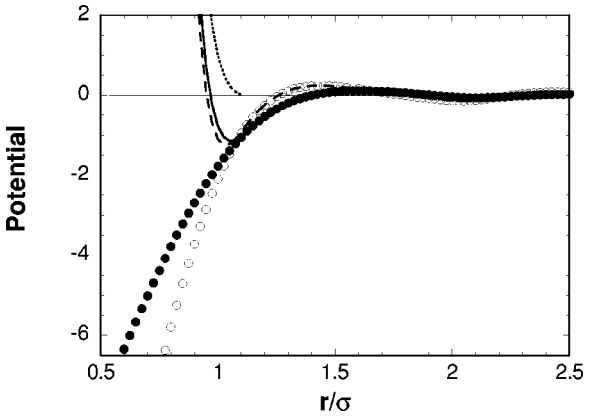

FIG. 2. The interaction potentials for $N = 200$ PRISM calculations. The dotted curve represents the purely repulsive (shifted Lennard-Jones) potential. The polymer–polymer component of the medium-induced interaction $W_{pp}(r)$ for a polymer melt and polymer in an infinitely dilute solution are shown with closed and open circles, respectively. The solid and dashed lines correspond to the sum of the repulsive and medium-induced potentials for the melt and dilute solutions cases.

III. RESULTS AND DISCUSSION

A. Intramolecular dimensions

The PRISM calculations on the repulsive reference system are performed at a total density of $0.85\sigma^{-3}$ at all concentrations of the polymer. To keep our model simple, we take $\sigma_{ss} = \sigma_{sp} = \sigma_{pp} = \sigma$ and $k_B T/\epsilon = 1$ ($\epsilon_{ss} = \epsilon_{sp} = \epsilon_{pp} = \epsilon$). To determine the solvation field strength K, we calculate the mean square end-to-end distance $\langle R^2_e \rangle$ as a function of chain length N for the infinitely dilute solution, a polymer melt, and a solution with 50% polymer concentration. For these three conditions, MD data is collected for a comparison with PRISM results. The solvation potential in Eq. (7) is calculated from self-consistent PRISM theory. In Fig. 2 we show $W_{pp}(r)$ for an infinitely dilute solution and polymer melt along with the total interaction potentials $u_{pp}(r) + W_{pp}(r)$. The solvation potential is mostly attractive, but oscillations occur due to packing of the polymer and solvent. $W_{pp}(r)$ eventually dampens to zero as r increases beyond 5σ. The total interaction potentials both have minima at r slightly greater than 1σ. In order to optimize the agreement between PRISM and MD data, the field strength K in Eq. (7) is set equal to 0.90. Larger values of $K \sim 1$ lead to chain collapse in a dilute solution, while smaller values of K give chain dimensions in the melt limit that are too large. In all our PRISM calculations shown in this paper K is maintained at 0.90.

It can be observed from Fig. 2 that the solvation potential, at distances less than $r = \sigma$, is more attractive for the dilute solution than for the polymer melt. This region of $W_{pp}(r)$ is not relevant, however, since the bare repulsive interactions U_E at short distances dominate the total potential that the polymer chain sees. At larger distances ($r > \sigma$) the solvation potential for the polymer melt is more attractive than for the dilute solution. Since the bare interactions are small for $r > \sigma$, the solvation potential controls the total site/site potential that the polymer chain feels at larger distances. Furthermore, it can be seen from the figure that the solvation

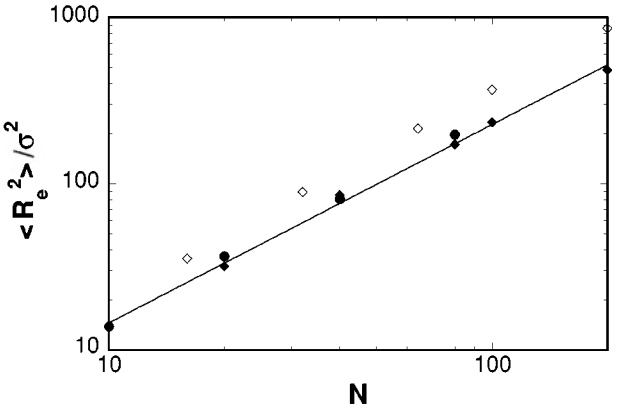

FIG. 3. $\langle R_e^2 \rangle$ vs N for the case of a polymer in an infinitely dilute solution. The line shown is a fit of the PRISM (closed diamonds) data. The closed circles are the results obtained from MD simulations run under the same conditions. The open diamonds are from MC simulations (Ref. 8) of a polymer in a vacuum (no solvent present).

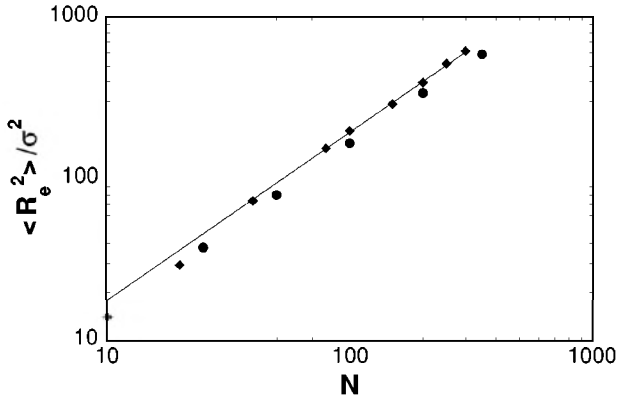

FIG. 4. A plot of $\langle R_e^2 \rangle$ vs N for the polymer melt case. A fit (excluding $N=10$ and 20) of the PRISM (diamonds) data is shown as the line . The results (Ref. 40) of the MD simulation for the polymer melt are the circles.

potential for the polymer melt decays to zero, and is less repulsive, at large distances than for the dilute solution. This is consistent with the notion that the excluded volume is "screened out" in the melt. Thus from an examination of Fig. 2, we conclude that a polymer chain in the melt would be predicted to be more compact than a corresponding macromolecule in a dilute solution. This is clearly seen when one examines $\langle R_e^2 \rangle$ as one proceeds from the dilute solution to the melt.

Figure 3 shows a logarithmic plot of the mean square end-to-end distance, $\langle R_e^2 \rangle$, versus the number of monomers, N, for an infinitely dilute solution. It can be seen that there is very good agreement between the PRISM theory predictions shown by the straight line and the MD simulations for $N=10$, 20, 40, and 80 denoted by the solid points (see Table I). In these MD simulations the solvent molecules are explicitly included. A power law fit $\langle R_e^2 \rangle > \propto N^{2\nu}$ of these data show that $\nu=0.59\pm0.07$ and 0.63 ± 0.06 for PRISM and MD simulations, respectively. The error bars here and throughout this paper represent 80% confidence limits. This is close to the approximately 3/5 value we expect for dilute solutions of a polymer in a good solvent. The open symbols in Fig. 3 are from MC simulations of Graessley and coworkers[8] on a polymer chain in a continuum. It can be seen that although the scaling is the same ($\nu=0.59$ for large N) the actual $\langle R_e^2 \rangle$ values are greater than 50% larger for a polymer in a continuum. So it appears that the monatomic solvent at the density studied is a poorer solvent for the polymer than a continuum solvent. This may not be surprising since density fluctuations are much smaller for the actual polymer solution than for a corresponding low density polymer. One might expect, therefore, that the polymer might reduce its chain dimensions in the less compressible medium. Previous studies[22,23] of the infinitely dilute solution using other integral equation approaches also found the chain dimensions to contract with increasing density of an athermal solvent. Gan and Eu[22] found $\nu=0.545$ whereas Taylor and Lipson[23] observed $\nu=0.58$ for the Flory exponent at high solvent packing fractions characteristic of a liquid.

TABLE I. MD simulation results.

N	Dilute solution $\langle R_e^2 \rangle$	50% polymer $\langle R_e^2 \rangle$	Melt (Ref. 40) $\langle R_e^2 \rangle$
10	13.86	13.71	
20	36.58	32.46	
25			37.9
40	80.64	67.39	
50			80.2
80	197.30	140.03	
100			167.0
200			340.0
350			590.0

Let us now consider the opposite extreme of the dense polymer melt. A logarithmic plot of $\langle R_e^2 \rangle$ versus N is shown in Fig. 4 for both the PRISM predictions and from MD simulations of Dunweg and coworkers[40] (see Table I). Data is shown for 10 to 350 monomeric units. Disregarding the $N=10$ and 20 data points from the PRISM data set, we obtain from a power law fit values of $\nu=0.52\pm0.04$ and 0.52 ± 0.02 for the PRISM and MD data, respectively, in close agreement with the value of 1/2 we expect for the polymer melt. Note that although the scaling is the same, PRISM theory predicts that the polymer chains are somewhat more swollen than for the simulation.

Single chain statistics are likewise obtained for a solution with a 50% concentration of polymers with $N=10-200$. As seen in Fig. 5, the scaling of $\langle R_e^2 \rangle$ with N is similar for both theory and simulation with $\nu=0.56\pm0.03$ and 0.55 ± 0.06 for PRISM and MD, respectively (see Table I). As with the polymer melt, we observe that the PRISM results exhibit chains that are somewhat more swollen than with simulation. In our self-consistent PRISM calculations we hold the strength of the solvation potential fixed. Obviously better agreement could have been achieved by allowing K to depend on concentration. Nevertheless, we feel that a reasonably accurate description of the intramolecular structure over the complete concentration range, with the correct scaling behavior, is obtained in our theory with K held fixed at 0.90.

We performed additional PRISM calculations as a function of concentration to observe how the chain contracts as the concentration increases from dilute solutions. These re-

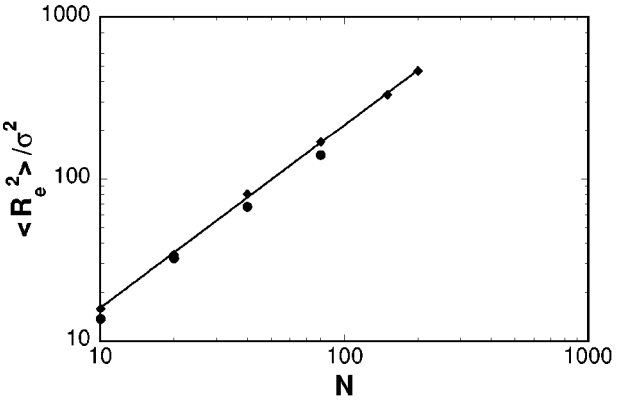

FIG. 5. $\langle R_e^2 \rangle$ vs N from MD simulations (circles) and PRISM calculations (diamonds) for a solution with 50% polymer. A linear fit of the PRISM data was performed and the resulting line is shown.

sults for $N=200$ are plotted in Fig. 6 on a logarithmic scale. It can be seen that there is evidence of a semidilute regime, where the chain dimensions contract with an approximate power law. The line in the figure is drawn with a slope of $-1/4$, suggesting that $\langle R_e^2 \rangle x^{-1/4}$ holds in the semidilute regime in accordance with scaling arguments.[5] It should be pointed out, however, that chains of $N=200$ may not be large enough to establish a well defined semidilute regime.

B. Intermolecular packing

The intermolecular radial distribution functions $g_{pp}(r)$, $g_{ss}(r)$, and $g_{sp}(r)$ completely describe the packing of polymer and solvent molecules in the mixture. Self-consistent PRISM and MD data are collected for a solution containing 50% polymer by volume. In Fig. 7 we compare these results for polymers chains with $N=80$. It can be seen from this figure that almost quantitative agreement is obtained between theory and simulation for both $g_{ss}(r)$ and $g_{ps}(r)$. For the correlations between polymer sites, however, significantly more structure in $g_{pp}(r)$ is predicted by PRISM theory than is actually present in the MD simulations. A contributing factor to this difference is that the chains are somewhat more extended (see Fig. 4) in the self-consistent PRISM calculation than in the MD simulation, resulting in a more intermolecular overlap of the polymer coils. This discrepancy in $g_{pp}(r)$ may also indicate that the direct correlation function between polymer sites at low concentrations is longer range than assumed in the Percus–Yevick closure.

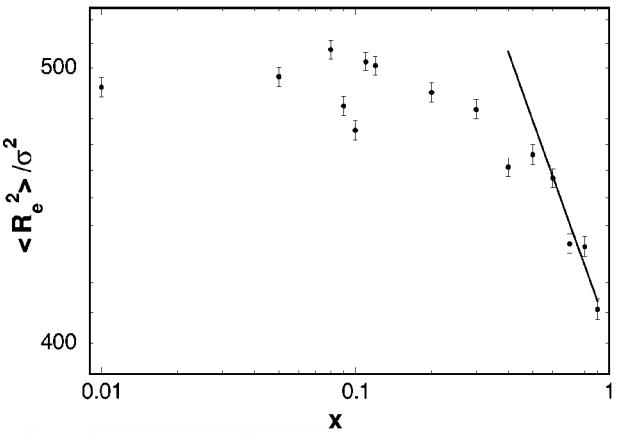

FIG. 6. A log–log plot of $\langle R_e^2 \rangle$ vs the fraction of polymer in solution, x. Results from PRISM calculations are represented by the circles. A line of slope $-1/4$ was drawn to show the transition to a semi-dilute regime.

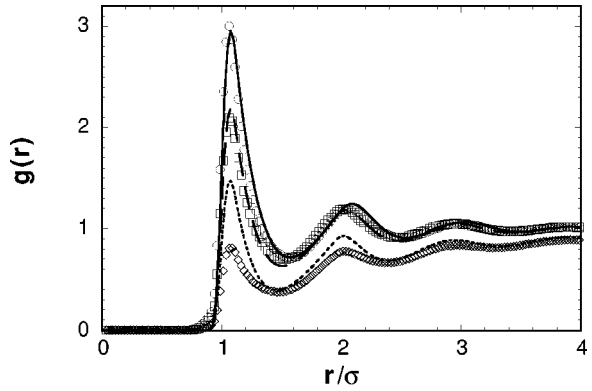

FIG. 7. Intermolecular radial distribution functions for a polymer with $N=80$ in a solution with 50% polymer obtained from PRISM calculations and MD simulations. The PRISM results are shown with curved lines: solid $g_{ss}(r)$, long-dash $g_{sp}(r)$, and short-dash $g_{pp}(r)$. The open symbols correspond to MD simulations: circles $g_{ss}(r)$, squares $g_{sp}(r)$, and diamonds $g_{pp}(r)$.

It is interesting to compare the PRISM predictions for intermolecular packing of the polymer in solution with the corresponding polymer in a continuum at the same polymer concentration. In Fig. 8 we plot $g_{pp}(r)$ for 80 unit chains at various concentrations. Both the polymer with explicit solvent molecules present and in a continuum solvent are shown for each site fraction x of the polymer. Note that there is considerably more structure in the polymer packing when the solvent molecules are included in the calculation. We know

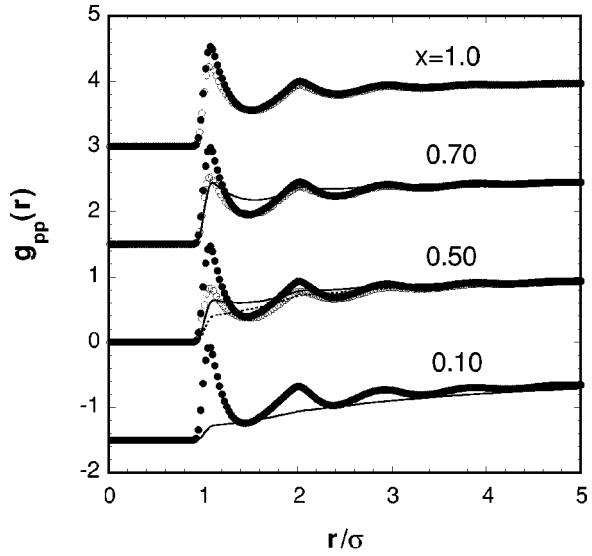

FIG. 8. The polymer/polymer radial distribution function $g_{pp}(r)$ for $N=80$ chains at various fractions x of polymer indicated in the figure. The solid circles refer to the results of PRISM calculations with solvent molecules included keeping the total density fixed at 0.85. The solid curves are the corresponding PRISM calculations with no solvent. The open circles correspond to results from MD simulations with a solvent present, while the dotted line is without a solvent. Some of the curves have been shifted along the y-axis for clarity.

that the monatomic solvent packs with strong peaks in the radial distribution function $g_{ss}(r)$ as seen in Fig. 7. It is not surprising, therefore, that the ordering of the solvent results in enhanced ordering in the polymer as well. Note also that the PRISM prediction for $g_{pp}(r)$ is remarkably insensitive to the concentration of the polymer when the solvent molecules are present in the calculation. Similar trends have been observed by Schweizer and coworkers[41] based on PRISM calculations that were not performed self-consistently. When the polymer is treated as a low density system without explicitly including the solvent molecules, however, $g_{pp}(r)$ near contact decreases and the correlation hole becomes of a longer range as the concentration is decreased.

In Fig. 8, we also show the results from MD simulations with and without a solvent present. The same trends are seen in the simulation, with the solvent inducing more ordering in the polymer, as predicted from self-consistent PRISM theory. It can also be seen that whereas PRISM theory predicts that $g_{pp}(r)$ is very weakly dependent on concentration, the MD simulation shows that the strength of the polymer/polymer correlations increases significantly with concentration. This is probably related to a longer range character in the direct correlation function as discussed above. From a comparison of the solid and dashed curves in Fig. 8, it can be seen that PRISM theory also predicts more structure in $g_{pp}(r)$ than when no solvent is present. This is not surprising since it is well known[12] that PRISM theory is most accurate at melt densities and becomes less reliable as the density is lowered. In the case we studied here, the monomer and the monatomic solvent had the same effective hard sphere diameter. In real polymer solutions, one might speculate that the multiplicity of length scales in actual solvent molecules might wash out some of the solvent-induced polymer packing seen in Figs. 7 and 8.

Throughout this work we assumed that the attractive interactions do not appreciably influence the packing of the polymer and solvent molecules. As a test of this hypothesis, we perform two sets of MD simulations on 20 unit chains in 50% solution. In the first simulation we employ the WCA repulsive potential from Eq. (5a) that we have used throughout this paper. In the second simulation we use the full Lennard-Jones potential including attractions. Figure 9 compares the intermolecular radial distribution functions from both simulations. It can be seen that indeed the attractive branch of the potential, defined in Eq. (5b), has only a minor affect on the structure of the polymer solution. As seen in the $N=80$ case at 50% concentration, we find that PRISM theory gives almost quantitative agreement with simulation for the solvent/solvent and solvent/polymer correlations, but overestimates the correlations between intermolecular polymer sites.

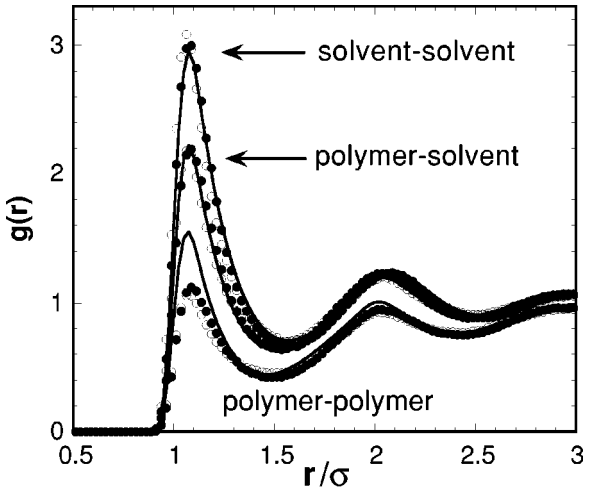

FIG. 9. The effect of attractions on the structure of polymer solutions for a 50% solution of $N=20$ unit chains with explicit solvent molecules present. Open symbols: MD without attractions; solid symbols: MD with attractions $\epsilon/k_BT=1.0$; curves: PRISM theory without attractions.

C. Phase behavior

We now use the structural information obtained on the purely repulsive reference system to estimate the phase behavior of the solution. Because of the apparent inaccuracy of PRISM theory predictions for $g_{pp}(r)$, and by inference $\hat{C}_{pp}(0)$, at low polymer concentrations, we expect the spinodal calculation to be only approximate. In order to compare our theory with Flory–Huggins theory, we first consider a model mixture with the attractive interactions as follows:

$$\epsilon_{pp}^{\text{att}}=\epsilon_{ss}^{\text{att}}=0;\ \epsilon_{sp}^{\text{att}}=-\epsilon, \tag{18}$$

so that solvent/polymer interactions are repulsive and demixing will occur at a sufficiently low temperature. Such a model was employed by Sariban and Binder[42] in their Monte Carlo simulations of blends. It is important to emphasize that this is not a conventional Lennard-Jones system since the solvent/polymer interactions are repulsive and Berthelot scaling clearly does not hold for this model. For simplicity we also keep the total density of the solution fixed and independent of temperature. We make an additional assumption that the direct correlation functions from the reference system $\hat{C}^0_{\alpha\gamma}(0)$, obtained at $k_BT/\epsilon=1$, can be used at other temperatures as well. Thus Eq. (13), together with the zero volume change on the mixing condition in Eq. (14), can be used to estimate the spinodal curve of this model solution.

The results are shown in Fig. 10 along with the corresponding Flory–Huggins prediction for this mixture. It can be seen that the PRISM calculations, which include nonrandom mixing and compressibility effects, predicts the solutions to be significantly more unstable than Flory–Huggins theory would predict. Whether T_S from PRISM theory is larger or smaller than from Flory–Huggins theory depends on the relative magnitudes of the athermal $\hat{C}^0_{\alpha\gamma}(0)$ from the reference system. An examination of Eqs. (13) and (16) indicates that the sign of the nonlinear term $\hat{C}_{pp}(0)\hat{C}_{ss}(0)-\hat{C}^2_{ps}(0)$, which turns out to be negative in our calculations, forces the PRISM spinodal curve to be above the corresponding Flory–Huggins spinodal. Moreover, it can be observed that PRISM theory predicts a stronger molecular weight dependence of the critical temperature than does Flory–Huggins theory.

As a final application of our theory, we consider the completely symmetric polymer solution defined by

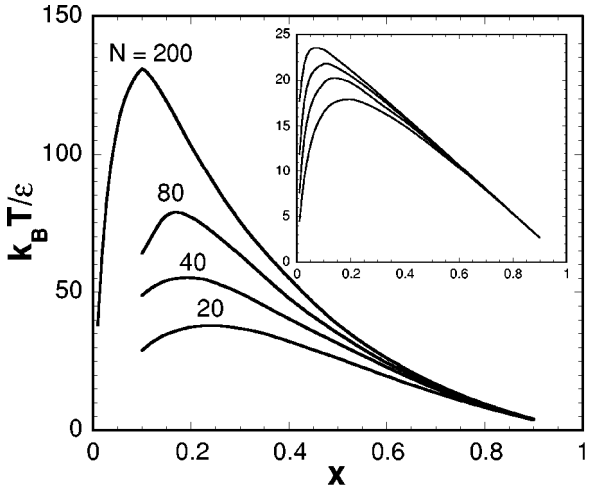

FIG. 10. Spinodal curves generated with the output of PRISM calculations for polymer solutions ($\epsilon_{pp}^{att}=\epsilon_{ss}^{att}=0$, $\epsilon_{sp}^{att}=-\epsilon$) for various values of N. The inset is the corresponding Flory–Huggins prediction under the same conditions. Note that the y-axis is $-k_B T/\epsilon_{sp}^{att}$ and, therefore, quantitatively different than the reduced temperature of conventional Lennard-Jones systems.

$$\epsilon_{pp}^{att}=\epsilon_{ss}^{att}=\epsilon_{sp}^{att}=\epsilon. \tag{19}$$

Clearly such a mixture would be predicted to be completely miscible in Flory–Huggins theory since the χ parameter, defined in Eq. (17), is zero. By contrast, as seen in Fig. 11, our prediction for this symmetric mixture shows that the solution is not completely miscible but instead appears to show an upper critical solution temperature (UCST). In this case the phase behavior is driven by nonrandom mixing and compressibility effects neglected in Flory–Huggins theory.

A similar solution was studied in the MC simulations of Gromov and coworkers[43] in the vicinity of the critical point ($k_B T_c/\epsilon=1.08, \rho_c\sigma^3=0.10$) of the pure solvent. For these state points they found a closed loop phase diagram with both LCST and UCST temperatures. In their case the existence of the LCST may have been due to the very high compressibility of the solvent near the critical point. At our mixture density of 0.85, we are well to the right of the critical point and it is not unreasonable that we see only the UCST. These results, however, are complicated by the fact that recent estimates[44] based on Wertheim's equation-of-state[45] suggest that at $\rho\sigma^3=0.85$ and $k_B T/\epsilon\approx 1$, the pure chain melt may be slightly within the gas/liquid coexistence region. Thus if there indeed is a UCST in the polymer solution, it may be unobservable because it may be preempted by the gas/liquid coexistence curve. In Fig. 12 we show a plot of the critical concentration ϕ_C from Fig. 11 as a function of chain length. It is interesting to note that the critical concentration scales as $\phi_C \sim N^{-1/2}$, as in Flory–Huggins theory, even though the Flory-Huggins χ parameter is zero for this solution.

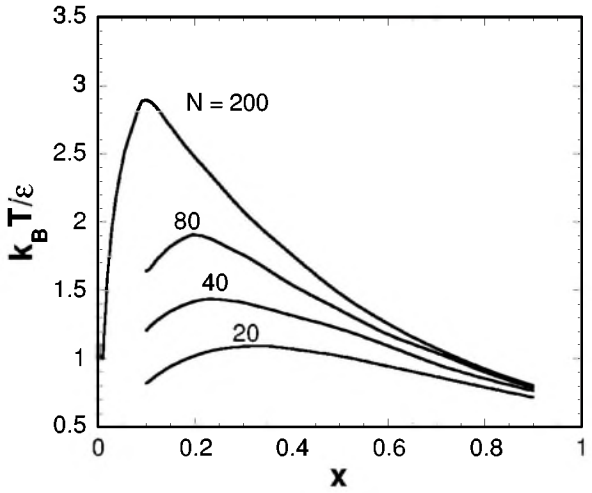

FIG. 11. Spinodal curves generated with an output of PRISM calculations for polymer solutions ($\epsilon_{pp}^{att}=\epsilon_{ss}^{att}=\epsilon_{sp}^{att}=\epsilon$) for various values of N.

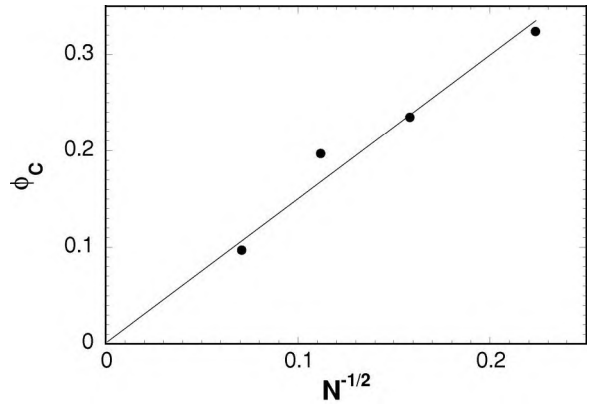

FIG. 12. Critical composition vs $N^{-1/2}$ for a polymer solution with $\epsilon_{pp}^{att}=\epsilon_{ss}^{att}=\epsilon_{sp}^{att}=\epsilon$. A linear fit of the data is shown.

IV. CONCLUSIONS

In this investigation we find that solvent packing effects can be incorporated into a theory of polymer solutions using self-consistent PRISM theory. Reasonable agreement is found with MD simulations using the solvation potential of Eq. (7) with an adjustable constant $K=0.90$ characterizing the overall strength of the solvation field. The effect of introducing the solvent explicitly into the calculation is to cause the chain to contract relative to chains in a continuum solvent at the same concentration. Approximately correct scaling of the mean square end-to-end distance with molecular weight is found over the complete concentration range from a dilute solution to the pure melt. Excellent agreement between theory and simulation is observed for the intermolecular pair correlations $g_{ss}(r)$ and $g_{sp}(r)$. PRISM theory is found to predict that the intermolecular polymer/polymer radial distribution function $g_{pp}(r)$ is only weakly dependent on concentration in contrast to MD simulation. Furthermore we observe from both theory and simulation that ordering of the solvent molecules tends to induce an additional structure in the polymer/polymer pair correlation function that is not present when the polymers are in a continuum solvent medium.

The phase behavior of the polymer solutions can be deduced from this theory using the RPA approximation for the effects of attractions on the direct correlation functions. In contrast to Flory–Huggins theory, this calculation accounts for compressibility and nonrandom mixing of polymer and

solvent. We find that a polymer solution characterized by symmetric energetics displayed UCST behavior, whereas Flory–Huggins theory would conclude that such a mixture was completely miscible. Future work will focus on MD simulations of this symmetric model to check these PRISM predictions.

Finally it should be emphasized that the PRISM calculations and MD simulations presented here were for a very idealized system consisting of completely flexible, tangent site chains, and monatomic solvent molecules of the same size as the monomers. Based on this model we observe significant departures in the polymer structure induced by the solvent. Moreover, strong deviations from Flory–Huggins theory are evident in the two example cases studied. By contrast, real polymers have more complex monomeric structure with significantly higher chain stiffness and the solvent molecules are obviously not simple monatomic entities with a single length scale. The question of whether the significant solvent-specific effects we have observed here are actually present in real polymer solutions will have to await future self- consistent PRISM and simulation studies using atomistic models.

ACKNOWLEDGMENTS

The authors would like to thank Professor K. S. Schweizer, Professor J. D. McCoy, and Dr. G. S. Grest for helpful discussions. The authors would also like to thank Dr. M. Muller for pointing out Ref. 44. Sandia is a multiprogram laboratory operated by Sandia Corporation, a Lockheed Martin Company for the U.S. Department of Energy under Contract No. DE-AC04094AL85000. Two of the authors (G.D.S. and D.B.) are thankful for the financial support provided by the National Science Foundation through grant DMR#0076303, as well as the University of Utah Center for Simulation of Accidental Fires and Explosions (C-SAFE) funded by the Department of Energy, Lawrence Livermore National Laboratory, under subcontract B341493.

[1] P. J. Flory, *Principles of Polymer Chemistry* (Cornell University Press, Ithaca, NY, 1953).
[2] H. Yamakawa, *Modern Theory of Polymer Solutions* (Harper & Rowe, New York, 1971).
[3] M. Doi and S. F. Edwards, *The Theory of Polymer Dynamics* (Clarendon, Oxford, 1986).
[4] M. Muthukumar and S. F. Edwards, J. Chem. Phys. **76**, 2720 (1982).
[5] P. G. De Gennes, *Scaling Concepts in Polymer Physics* (Cornell University Press, Ithaca, NY, 1979).
[6] F. T. Wall and F. Mandel, J. Chem. Phys. **63**, 4592 (1975).
[7] J. G. Curro, J. Chem. Phys. **61**, 1203 (1974).
[8] W. W. Graessley, R. C. Hayward, and G. S. Grest, Macromolecules **32**, 3510 (1999).
[9] B. Dünweg and K. Kremer, J. Chem. Phys. **99**, 6983 (1993).
[10] J. K. C. Suen, F. A. Escobedo, and J. J. dePablo, J. Chem. Phys. **106**, 1288 (1997); G. Luna Barcenas, D. G. Gromov, J. C. Meredith, I. C. Sanchez, J. J. de Pablo, and K. P. Johnston, Chem. Phys. Lett. **278**, 302 (1997); P. Ahlrichs and B. Dünweg, J. Chem. Phys. **111**, 8225 (1999).
[11] G. D. Smith, D. Bedrov, and O. Borodin, Phys. Rev. Lett. **85**, 5583 (2000); G. D. Smith, D. Bedrov, and O. Borodin, J. Am. Chem. Soc. **122**, 9548 (2000).
[12] For recent reviews see K. S. Schweizer and J. G. Curro, Adv. Polym. Sci. **116**, 321 (1994); K. S. Schweizer and J. G. Curro, Adv. Chem. Phys. **98**, 1 (1997).
[13] J. D. Weinhold, J. G. Curro, A. Habenschuss, and J. D. Londono, Macromolecules **32**, 7276 (1999).
[14] M. Pütz, J. G. Curro, and G. S. Grest, J. Chem. Phys. **114**, 2847 (2001).
[15] J. J. Rajasekaran, J. G. Curro, and J. D. Honeycutt, Macromolecules **28**, 6843 (1995).
[16] T. C. Clancy, M. Pütz, J. D. Weinhold, J. G. Curro, and W. L. Mattice, Macromolecules **33**, 9452 (2000).
[17] J. Melenkevitz, J. G. Curro, and K. S. Schweizer, J. Chem. Phys. **99**, 5571 (1993).
[18] K. S. Schweizer, K. G. Honnell, and J. G. Curro, J. Chem. Phys. **96**, 3211 (1992).
[19] C. J. Grayce, A. Yethiraj, and K. S. Schweizer, J. Chem. Phys. **100**, 6857 (1994).
[20] P. G. Khalatur and A. R. Khokhlov, Mol. Phys. **93**, 555 (1998).
[21] P. G. Khalatur, L. V. Zherenkova, and A. R. Khokhlov, Eur. Phys. J. B **5**, 881 (1998).
[22] H. H. Gan and B. C. Eu, J. Chem. Phys. **109**, 2011 (1998).
[23] M. P. Taylor and J. E. G. Lipson, Fluid Phase Equilib. **150–151**, 641 (1998).
[24] K. S. Schweizer and J. G. Curro, Phys. Rev. Lett. **58**, 246 (1987).
[25] J. G. Curro and K. S. Schweizer, Macromolecules **20**, 1928 (1987).
[26] J. G. Curro and K. S. Schweizer, J. Chem. Phys. **87**, 1842 (1987).
[27] D. Chandler and H. C. Andersen, J. Chem. Phys. **57**, 1930 (1972).
[28] D. Chandler, in *Studies in Statistical Mechanics VIII*, edited by E. W. Montroll and J. L. Lebowitz (North-Holland, Amsterdam, 1982).
[29] J. P. Hansen and I. R. McDonald, *Theory of Simple Liquids* (Academic Press, London, 1986).
[30] J. D. Weeks, D. Chandler, and H. C. Andersen, J. Chem. Phys. **54**, 5237 (1971).
[31] D. Chandler, Y. Singh, and D. M. Richardson, J. Chem. Phys. **81**, 1975 (1984).
[32] A. L. Nichols, D. Chandler, Y. Singh, and D. M. Richardson, J. Chem. Phys. **81**, 5109 (1984).
[33] N. Metropolis, A. W. Rosenbluth, M. N. Rosenbluth, A. H. Teller, and A. Teller, J. Chem. Phys. **21**, 1087 (1953).
[34] J. B. Hooper, J. D. McCoy, and J. G. Curro, J. Chem. Phys. **112**, 3090 (2000).
[35] J. G. Curro and K. S. Schweizer, Macromolecules **24**, 6736 (1991).
[36] J. D. McCoy, M. A. Teixeira, and J. G. Curro, J. Chem. Phys. **114**, 4289 (2001).
[37] J. G. Kirkwood and F. P. Buff, J. Chem. Phys. **19**, 774 (1951).
[38] J. Ryckaert, G. Ciccotti, and H. J. C. Berendsen, J. Comput. Phys. **23**, 327 (1977).
[39] G. J. Martyna, M. E. Tuckerman, D. J. Tobias, and M. L. Klein, Mol. Phys. **87**, 1117 (1996).
[40] B. Dunweg, G. S. Grest, and K. Kremer, "Molecular dynamics simulations of polymer systems," in *Numerical Methods for Polymeric Systems*, IMA Volumes in Mathematics and its Applications, edited by S. Whittington (Springer-Verlag, New York, 1998), Vol. 102, p. 159; M. Pütz, Ph.D. thesis, University of Mainz, Germany, 1999.
[41] K. S. Schweizer and A. P. Chaterjee, private communication.
[42] A. Sariban and K. Binder, J. Chem. Phys. **86**, 5859 (1987).
[43] D. G. Gromov, J. J. de Pablo, G. Luna-Barcenas, I. C. Sanchez, and K. P. Johnston, J. Chem. Phys. **108**, 4647 (1998).
[44] L. Gonzalez MacDowell, M. Muller, C. Vega, and K. Binder, J. Chem. Phys. **113**, 419 (2000).
[45] M. S. Wertheim, J. Chem. Phys. **87**, 7323 (1987).